Advances in Nano Research, *Vol. 14, No. 3 (2023) 261-271*
https://doi.org/10.12989/anr.2023.14.3.261

Thermal buckling of rectangular sandwich plates with advanced hybrid SMA/CNT/graphite/epoxy composite face sheets

Saeed Kamarian and Jung-Il Song*

Department of Mechanical Engineering, Changwon National University, Changwon, South Korea

(*Received April 7, 2022, Revised May 18, 2022, Accepted June 17, 2022*)

Abstract. The present study follows three main goals. First, an analytical solution with high accuracy is developed to assess the effects of embedding pre-strained shape memory alloy (SMA) wires on the critical buckling temperatures of rectangular sandwich plates made of soft core and graphite fiber/epoxy (GF/EP) face sheets based on piecewise low-order shear deformation theory (PLSDT) using Brinson's model. As the second goal, this study compares the effects of SMAs on the thermal buckling of sandwich plates with those of carbon nanotubes (CNTs). The glass transition temperature is considered as a limiting factor. For each material, the effective ranges of operating temperature and thickness ratio are determined for real situations. The results indicate that depending on the geometric parameters and thermal conditions, one of the SMAs and CNTs may outperform the other. The third purpose is to study the thermal buckling of sandwich plates with advanced hybrid SMA/CNT/GF/EP composite face sheets. It is shown that in some circumstances, the co-incorporation of SMAs and CNTs leads to an astonishing enhancement in the critical buckling temperatures of sandwich plates.

Keywords: advanced hybrid composites; analytical solution; carbon nanotubes; sandwich plates; shape memory alloys; thermal buckling

1. Introduction

The extraordinary features of sandwich structures, especially their high strength-to-weight ratio, have attracted the attention of various industries including aerospace, marine, civil, automotive, railway, and sport (Birman and Kardomateas 2018). Depending on their applications, these structures may be exposed to thermal environments (Mekerbi *et al*. 2021, Daikh *et al.* 2021), which may even buckle due to the thermal stresses (Watanabe *et al.* 1997, Babu and Kant 2000). Therefore, the analysis of the stability of sandwich structures under thermal environments is of great importance. The authors (Kamarian *et al.* 2020) showed three main approaches to delay thermal buckling phenomenon in composite structures: 1) using materials like SMAs to generate tensile stress to counteract the compressive thermal stresses, 2) application of materials like CNTs to change the thermo-mechanical properties of composites, and 3) design optimization (like stacking sequence optimization) of composite structures. Regarding the first two strategies, choosing the right type and amount of materials is of crucial significance.

SMAs are advanced materials capable of recovering large strains without plastic deformation, as well as producing tensile stress if prevented from returning to their general state (Brinson 1993). These two outstanding properties have encouraged the use of SMAs to enhance the performance of structures (Lecce and Concilio 2015, Bhaskar *et al.* 2020). Concerning heat-exposed sandwich structures, Asadi *et al*. (2015) developed an analytical method to examine the thermal stability of sandwich cylindrical shells containing SMA wires. Katariya *et al.* (2017) used the finite element method (FEM) to assess the effect of SMAs on the thermal buckling of sandwich shell panels. Nejati *et al*. (2019) also analytically examined the thermal vibration of SMA hybrid composite double curved sandwich panels based on first-order shear deformation theory (FSDT). Lal and Markad (2021) studied the thermal post-buckling of smart sandwich plates with the incorporation of SMAs and shape memory polymers (SMPs). The critical buckling temperatures were obtained based on a higher-order shear deformation theory (HSDT) using FEM.

CNTs are a class of advanced materials with exceptional properties and wide applications, especially in composite structures (Garg *et al.* 2021, Bendenia, 2020). Even small amounts of CNTs can significantly enhance the thermo-mechanical properties of the composites (Siddiqui *et al.* 2010, Barai and Weng, 2011, Kamarian *et al.* 2021a). Over the last decade, the effects of CNTs on the behavior of composite structures have been extensively explored. Among them, some studies deal with the influence of CNTs on the thermal buckling of sandwich structures. Sankar *et al*. (2017) investigated the nonlinear dynamic thermal buckling of sandwich spherical and conical shells with CNT-reinforced face sheets. Ebrahimia and Farazmandnia (2018) examined the buckling of functionally graded CNT-reinforced sandwich beams under thermal loads. Mehar *et al*. (2019) evaluated the thermal buckling of graded CNT-reinforced composite sandwich shells based on a higher-order shear deformation theory (HSDT). Tung and long (2019) assessed the buckling and post-buckling of CNT-

*Corresponding author, Professor,
E-mail: jisong@changwon.ac.kr

ISSN: 2287-237X (Print), 2287-2388 (Online)

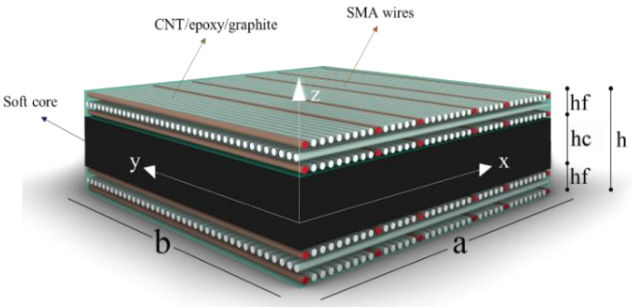

Fig. 1 Schematic of a soft-core sandwich plate with advanced hybrid SMA/CNT/GF/EP composite face sheets

reinforced cylindrical sandwich panels under thermo-mechanical loadings. Kamarian *et al*. (2021b) evaluated the role of CNTs in the variations of critical buckling temperatures of sandwich plates. Based on Reddy's HSDT and by using the Galerkin and Runge-Kutta methods, Dat *et al*. (2021) investigated the nonlinear thermal dynamic buckling and global optimization of smart sandwich plates composed of a porous homogeneous core, two CNT-reinforced intermediate composite layers, and two piezoelectric face sheets.

In the continuation of the authors' previous studies (Kamarian *et al.* 2020, Kamarian and Song, 2022), the present work is mainly aimed to investigate the effects of two advanced materials, namely SMAs and CNTs, on the critical buckling temperature of sandwich plates. Based on PLSDT and using Brinson's model, the thermal buckling of sandwich plates with SMA hybrid composite face sheets is first studied using an analytical solution. Then, the performances of SMA wires and CNTs in enhancing the buckling temperature of sandwich plates are compared. Moreover, the thermal stability of sandwich plates composed of advanced hybrid SMA/CNT-reinforced face sheets is examined.

2. Governing equations

Consider a rectangular sandwich plate made of an aluminum core and GF/EP composite face sheets, as shown in Fig. 1. The face sheets may be reinforced with CNTs or SMA wires. As observed, h_f, h_c, h, a and b denote the face sheet thickness, core thickness, total thickness, length, and width, respectively.

According to PLSDT (Li 2015, 2018), the displacement components of the sandwich structure are expressed as:

$$\begin{aligned}
&w(x,y,z,t) = w\\
&u_t(x,y,z,t) = -\frac{\hbar_c+\hbar_f}{2}\psi_1 - (z-\frac{\hbar_c+\hbar_f}{2})\frac{\partial w}{\partial x}\\
&u_b(x,y,z,t) = +\frac{\hbar_c+\hbar_f}{2}\psi_1 - (z+\frac{\hbar_c+\hbar_f}{2})\frac{\partial w}{\partial x}\\
&u_c(x,y,z,t) = -z(\frac{\hbar_c+\hbar_f}{\hbar_c}\psi_1 - \frac{\hbar_f}{\hbar_c}\frac{\partial w}{\partial x})
\end{aligned} \tag{1}$$

$$\begin{aligned}
&v_t(x,y,z,t) = -\frac{\hbar_c+\hbar_f}{2}\psi_2 - (z-\frac{\hbar_c+\hbar_f}{2})\frac{\partial w}{\partial y}\\
&v_b(x,y,z,t) = +\frac{\hbar_c+\hbar_f}{2}\psi_2 - (z+\frac{\hbar_c+\hbar_f}{2})\frac{\partial w}{\partial y}\\
&v_c(x,y,z,t) = -z(\frac{\hbar_c+\hbar_f}{\hbar_c}\psi_2 - \frac{\hbar_f}{\hbar_c}\frac{\partial w}{\partial y})
\end{aligned}$$

where, *t*, *b* and *c* indices stand for the top face sheet, bottom face sheet, and core, respectively. Furthermore, ψ_1 and ψ_2 show the rotation angles of the straight line that connects the midpoint of the face sheets in xoz and yoz planes, respectively. The strain-displacement relations may be expressed as:

$$\begin{aligned}
&\varepsilon_{tx} = \frac{\partial u_t}{\partial x}\\
&= \left(-\frac{\hbar_c+\hbar_f}{2}\frac{\partial\psi_1}{\partial x}\right) + \left(z-\frac{\hbar_c+\hbar_f}{2}\right)\left(-\frac{\partial^2 w}{\partial x^2}\right)\\
&\varepsilon_{ty} = \frac{\partial v_t}{\partial y}\\
&= \left(-\frac{\hbar_c+\hbar_f}{2}\frac{\partial\psi_2}{\partial y}\right) + \left(z-\frac{\hbar_c+\hbar_f}{2}\right)\left(-\frac{\partial^2 w}{\partial y^2}\right)\\
&\gamma_{txy} = \frac{\partial u_t}{\partial y} + \frac{\partial v_t}{\partial x}\\
&= \left(-\left(\frac{\hbar_c+\hbar_f}{2}\right)\left(\frac{\partial\psi_1}{\partial y}+\frac{\partial\psi_2}{\partial x}\right)\right) + \left(z-\frac{\hbar_c+\hbar_f}{2}\right)\left(-2\frac{\partial^2 w}{\partial x\partial y}\right)\\
&\varepsilon_{bx} = \frac{\partial u_b}{\partial x} = \left(\frac{\hbar_c+\hbar_f}{2}\frac{\partial\psi_1}{\partial x}\right) + \left(z+\frac{\hbar_c+\hbar_f}{2}\right)\left(-\frac{\partial^2 w}{\partial x^2}\right)\\
&\varepsilon_{by} = \frac{\partial v_b}{\partial y}\\
&= \left(\frac{\hbar_c+\hbar_f}{2}\frac{\partial\psi_2}{\partial y}\right) + \left(z+\frac{\hbar_c+\hbar_f}{2}\right)\left(-\frac{\partial^2 w}{\partial y^2}\right)\\
&\gamma_{bxy} = \frac{\partial u_b}{\partial y} + \frac{\partial v_b}{\partial x}\\
&= \left((\frac{\hbar_c+\hbar_f}{2})(\frac{\partial\psi_1}{\partial y}+\frac{\partial\psi_2}{\partial x})\right) + \left(z+\frac{\hbar_c+\hbar_f}{2}\right)\left(-2\frac{\partial^2 w}{\partial x\partial y}\right)
\end{aligned} \tag{2}$$

Similarly, the linear strain components of the core may be written as:

$$\begin{aligned}
&\varepsilon_{cx} = \frac{\partial u_c}{\partial x} = z\left(-\frac{\hbar_c+\hbar_f}{\hbar_c}\frac{\partial\psi_1}{\partial x} + \frac{\hbar_f}{\hbar_c}\frac{\partial^2 w}{\partial x^2}\right)\\
&\varepsilon_{cy} = \frac{\partial v_c}{\partial y} = z\left(-\frac{\hbar_c+\hbar_f}{\hbar_c}\frac{\partial\psi_2}{\partial y} + \frac{\hbar_f}{\hbar_c}\frac{\partial^2 w}{\partial y^2}\right)\\
&\gamma_{cxy} = \frac{\partial u_c}{\partial y} + \frac{\partial v_c}{\partial x}\\
&= z\left(-\frac{\hbar_c+\hbar_f}{\hbar_c}(\frac{\partial\psi_1}{\partial y}+\frac{\partial\psi_2}{\partial x}) + \frac{\hbar_f}{\hbar_c}(2\frac{\partial^2 w}{\partial x\partial y})\right)\\
&\gamma_{cxz} = \frac{\partial u_c}{\partial z} + \frac{\partial w}{\partial x} = \frac{\hbar_c+\hbar_f}{\hbar_c}\left(\frac{\partial w}{\partial x} - \psi_1\right)\\
&\gamma_{cyz} = \frac{\partial v_c}{\partial z} + \frac{\partial w}{\partial y} = \frac{\hbar_c+\hbar_f}{\hbar_c}\left(\frac{\partial w}{\partial y} - \psi_2\right)
\end{aligned} \tag{3}$$

The governing stability equations in the present study are obtained using energy method (Reddy 2003).

$$\delta(W-U)=0 \tag{4}$$

where U and W represent the total strain energy and the total work of external loads. It should be noted that the effects of thermal stresses as well as the recovery stresses appear as external load work in the present study. Therefore, the stress components in the k^{th} layer of the face sheets and core can be defined by:

$$\begin{Bmatrix}\sigma_{tx}\\ \sigma_{ty}\\ \tau_{txy}\end{Bmatrix}^{kt}=\begin{bmatrix}\bar{Q}_{11} & \bar{Q}_{12} & \bar{Q}_{16}\\ & \bar{Q}_{22} & \bar{Q}_{26}\\ Sym & & \bar{Q}_{66}\end{bmatrix}^{kt}\begin{Bmatrix}\varepsilon_{tx}\\ \varepsilon_{ty}\\ \gamma_{txy}\end{Bmatrix}^{kt},$$
$$\begin{Bmatrix}\sigma_{bx}\\ \sigma_{by}\\ \tau_{bxy}\end{Bmatrix}^{kb}=\begin{bmatrix}\bar{Q}_{11} & \bar{Q}_{12} & \bar{Q}_{16}\\ & \bar{Q}_{22} & \bar{Q}_{26}\\ Sym & & \bar{Q}_{66}\end{bmatrix}^{kb}\begin{Bmatrix}\varepsilon_{bx}\\ \varepsilon_{by}\\ \gamma_{bxy}\end{Bmatrix}^{kb} \tag{5}$$
$$\begin{Bmatrix}\sigma_{cx}\\ \sigma_{cy}\\ \tau_{cxy}\end{Bmatrix}^{kc}=\begin{bmatrix}\bar{Q}_{11} & \bar{Q}_{12} & \bar{Q}_{16}\\ & \bar{Q}_{22} & \bar{Q}_{26}\\ Sym & & \bar{Q}_{66}\end{bmatrix}^{kc}\begin{Bmatrix}\varepsilon_{cx}\\ \varepsilon_{cy}\\ \gamma_{cxy}\end{Bmatrix}^{kc},$$
$$\begin{Bmatrix}\tau_{cyz}\\ \tau_{cxz}\end{Bmatrix}^{kc}=\begin{bmatrix}\bar{Q}_{44} & \bar{Q}_{45}\\ \bar{Q}_{45} & \bar{Q}_{55}\end{bmatrix}\begin{Bmatrix}\gamma_{yz}\\ \gamma_{xz}\end{Bmatrix}^{kc}$$

where $\overline{Q}_{ij}$ denote the reduced stiffness coefficients (Reddy 2003). Moreover, *kt*, *kb*, and *kc* denote the k^{th} layer in top face sheet, bottom face sheet, and the core, respectively. The strain energy of the structures is obtained as follows

$$\begin{aligned}
&U=U_t+U_b+U_c\\
&U_t=U_{tx}+U_{ty}+U_{txy}\\
&=\frac{1}{2}\int_0^a\int_0^b\int_{\frac{\hbar_c}{2}}^{\frac{\hbar_c}{2}+\hbar_f}\sigma_{tx}\varepsilon_{tx}dzdydx\\
&+\frac{1}{2}\int_0^a\int_0^b\int_{\frac{\hbar_c}{2}}^{\frac{\hbar_c}{2}+\hbar_f}\sigma_{ty}\varepsilon_{ty}dzdydx\\
&+\int_0^a\int_0^b\int_{\frac{\hbar_c}{2}}^{\frac{\hbar_c}{2}+\hbar_f}\tau_{txy}\gamma_{txy}dzdydx\\
&U_b=U_{bx}+U_{by}+U_{bxy}\\
&=\frac{1}{2}\int_0^a\int_0^b\int_{-\frac{\hbar_c}{2}-\hbar_f}^{-\frac{\hbar_c}{2}}\sigma_{bx}\varepsilon_{bx}dzdydx\\
&+\frac{1}{2}\int_0^a\int_0^b\int_{-\frac{\hbar_c}{2}-\hbar_f}^{-\frac{\hbar_c}{2}}\sigma_{by}\varepsilon_{by}dzdydx\\
&+\int_0^a\int_0^b\int_{-\frac{\hbar_c}{2}-\hbar_f}^{-\frac{\hbar_c}{2}}\tau_{bxy}\gamma_{bxy}dzdydx\\
&U_c=U_{cx}+U_{cy}+U_{cxy}+U_{cxz}+U_{cyz}\\
&=\frac{1}{2}\int_0^a\int_0^b\int_{-\frac{\hbar_c}{2}}^{\frac{\hbar_c}{2}}\sigma_{cx}\varepsilon_{cx}dzdydx\\
&+\frac{1}{2}\int_0^a\int_0^b\int_{-\frac{\hbar_c}{2}}^{\frac{\hbar_c}{2}}\sigma_{cy}\varepsilon_{cy}dzdydx\\
&+\int_0^a\int_0^b\int_{-\frac{\hbar_c}{2}}^{\frac{\hbar_c}{2}}\tau_{cxy}\gamma_{cxy}dzdydx\\
&+\int_0^a\int_0^b\int_{-\hbar_c/2}^{\hbar_c/2}\tau_{cxz}\gamma_{cxz}dzdydx\\
&+\int_0^a\int_0^b\int_{-\hbar_c/2}^{\hbar_c/2}\tau_{cyz}\gamma_{cyz}dzdydx
\end{aligned} \tag{6}$$

The total work done by the external loads (thermal stress and recovery stress) can be calculated by:

$$\begin{aligned}
&W=W_{thermal}+W_{recovery}\\
&W_{thermal}=\int_0^a\int_0^b\left(-N_x^T\frac{\partial^2 w}{\partial x^2}-N_y^T\frac{\partial^2 w}{\partial x^2}\right)\\
&W_{recovery}=\int_0^a\int_0^b\left(N_x^r\frac{\partial^2 w}{\partial x^2}+N_y^r\frac{\partial^2 w}{\partial x^2}\right)
\end{aligned} \tag{7}$$

where the thermal forces ($N_x^T$and N_y^T) and the recovery forces (N_x^r and N_y^r) are defined as follows:

$$\begin{aligned}
&\begin{pmatrix}N_x^T\\ N_y^T\end{pmatrix}=\begin{pmatrix}N_{cx}^T\\ N_{cy}^T\end{pmatrix}+\begin{pmatrix}N_{tx}^T\\ N_{ty}^T\end{pmatrix}+\begin{pmatrix}N_{bx}^T\\ N_{by}^T\end{pmatrix}\\
&=\begin{pmatrix}N_{cx}^T\\ N_{cy}^T\end{pmatrix}+2\begin{pmatrix}N_{fx}^T\\ N_{fy}^T\end{pmatrix}\begin{pmatrix}N_x^r\\ N_y^r\end{pmatrix}=\begin{pmatrix}N_{tx}^r\\ N_{ty}^r\end{pmatrix}+\begin{pmatrix}N_{bx}^r\\ N_{by}^r\end{pmatrix}\\
&=2\begin{pmatrix}N_{fx}^r\\ N_{fy}^r\end{pmatrix}
\end{aligned} \tag{8}$$

in which

$$\begin{aligned}
&\begin{Bmatrix}N_{fx}^T\\ N_{fy}^T\end{Bmatrix}=\int_{\frac{\hbar_c}{2}}^{\frac{\hbar_c}{2}+\hbar_f}\begin{bmatrix}\bar{Q}_{11} & \bar{Q}_{12}\\ \bar{Q}_{12} & \bar{Q}_{22}\end{bmatrix}_{face}\begin{Bmatrix}\alpha_x\\ \alpha_y\end{Bmatrix}_{face}\Delta T\ dz\\
&=\int_{-\frac{\hbar_c}{2}-\hbar_f}^{-\frac{\hbar_c}{2}}\begin{bmatrix}\bar{Q}_{11} & \bar{Q}_{12}\\ \bar{Q}_{12} & \bar{Q}_{22}\end{bmatrix}_{face}\begin{Bmatrix}\alpha_x\\ \alpha_y\end{Bmatrix}_{face}\Delta T\ dz\\
&\begin{Bmatrix}N_{cx}^T\\ N_{cy}^T\end{Bmatrix}=\int_{-\frac{\hbar_c}{2}}^{\frac{\hbar_c}{2}}\begin{bmatrix}\bar{Q}_{11} & \bar{Q}_{12}\\ \bar{Q}_{12} & \bar{Q}_{22}\end{bmatrix}_{core}\begin{Bmatrix}\alpha_x\\ \alpha_y\end{Bmatrix}_{core}\Delta T\ dz\\
&\begin{Bmatrix}N_{fx}^r\\ N_{fy}^r\end{Bmatrix}=\int_{\frac{\hbar_c}{2}}^{\frac{\hbar_c}{2}+\hbar_f}V_s\sigma^r\begin{Bmatrix}cos^2(\theta)\\ sin^2(\theta)\end{Bmatrix}_{face}dz\\
&=\int_{-\hbar_c/2-\hbar_f}^{-\hbar_c/2}V_s\sigma^r\begin{Bmatrix}cos^2(\theta)\\ sin^2(\theta)\end{Bmatrix}_{face}dz
\end{aligned} \tag{9}$$

where α_{ij},ΔT,V_s and θrepresent the coefficient thermal expansion, temperature difference relative to the reference temperature (T_{ref}), SMA volume fraction, and the angle that the graphite fibers and SMA wires make with *x*-directions, respectively (Asadi *et al.* 2014). Additionally, σ^r represents the tensile recovery stress generated by SMA wires which is briefly described in Appendix 1, based on the Brinson's model (Brinson 2003). Note that the embedded SMA wires ae considered to be aligned parallel to the longitudinal direction of the graphite fibers (Tsoi *et al.* 2003). By inserting Eqs. (6) and (7) in to Eq. (4), the thermal buckling equations may be obtained. For the case that the temperature is uniformly distributed in the structure, and the top and bottom faces sheets are similar cross-ply laminates, the governing equations take the following form:

$$-g_{11}^{(3)}\frac{\partial^4 w}{\partial x^4}-\left(2g_{12}^{(3)}+4g_{66}^{(3)}\right)\frac{\partial^4 w}{\partial x^2\partial y^2}-g_{22}^{(3)}\frac{\partial^4 w}{\partial y^4}+g_{11}^{(2)}\frac{\partial^3\psi_1}{\partial x^3} \tag{10}$$

$$+\left(g_{12}^{(2)}+2g_{66}^{(2)}\right)\left(\frac{\partial^3\psi_1}{\partial x\partial y^2}+\frac{\partial^3\psi_2}{\partial x^2\partial y}\right)+g_{22}^{(2)}\frac{\partial^3\psi_2}{\partial y^3}$$
$$+S_{cxz}\left(\frac{\partial^2 w}{\partial x^2}-\frac{\partial\psi_1}{\partial x}\right)+S_{cyz}\left(\frac{\partial^2 w}{\partial y^2}-\frac{\partial\psi_2}{\partial y}\right)+\left(N_x^r-N_x^T\right)\frac{\partial^2 w}{\partial x^2}$$
$$+\left(N_y^r-N_y^T\right)\frac{\partial^2 w}{\partial y^2}=0$$
$$-g_{11}^{(2)}\frac{\partial^3 w}{\partial x^3}-\left(g_{12}^{(2)}+2g_{66}^{(2)}\right)\frac{\partial^3 w}{\partial x\partial y^2}+\left(g_{12}^{(1)}+g_{66}^{(1)}\right)\frac{\partial^2\psi_2}{\partial x\partial y}+$$
$$g_{11}^{(1)}\frac{\partial^2\psi_1}{\partial x^2}+g_{66}^{(1)}\frac{\partial^2\psi_1}{\partial y^2}+S_{cxz}\left(\frac{\partial w}{\partial x}-\psi_1\right)=0$$
$$-g_{22}^{(2)}\frac{\partial^3 w}{\partial y^3}-\left(g_{12}^{(2)}+2g_{66}^{(2)}\right)\frac{\partial^3 w}{\partial x^2\partial y}+\left(g_{12}^{(1)}+g_{66}^{(1)}\right)\frac{\partial^2\psi_1}{\partial x\partial y}$$
$$+g_{22}^{(1)}\frac{\partial^2\psi_2}{\partial y^2}+g_{66}^{(1)}\frac{\partial^2\psi_2}{\partial x^2}+S_{cyz}\left(\frac{\partial w}{\partial y}-\psi_2\right)=0$$

where the coefficients of $g_{ij}^{(k)}$ are presented in Appendix 2. Note that, the SMA wires are assumed to be embedded only in the face sheets. In cases where the core is reinforced with SMA wires, the recovery force generated in the core needs to be considered. The related boundary conditions are also derived as follows

$$x=0,\quad a:\begin{cases}\delta w=0\\ or\left(\begin{matrix}g_{11}^{(2)}\frac{\partial^2\psi_1}{\partial x^2}-g_{11}^{(3)}\frac{\partial^3 w}{\partial x^3}+g_{12}^{(2)}\frac{\partial^2\psi_2}{\partial x\partial y}-g_{12}^{(3)}\frac{\partial^3 w}{\partial x\partial y^2}\\ +S_{cxz}\left(\frac{\partial w}{\partial x}-\psi_1\right)\end{matrix}\right)=0\\ \delta\left(\frac{\partial w}{\partial x}\right)=0\\ or\left(-g_{11}^{(2)}\frac{\partial\psi_1}{\partial x}+g_{11}^{(3)}\frac{\partial^2 w}{\partial x^2}-g_{12}^{(2)}\frac{\partial\psi_2}{\partial y}+g_{12}^{(3)}\frac{\partial^2 w}{\partial y^2}\right)=0\\ \delta\psi_1=0\\ or\left(g_{11}^{(1)}\frac{\partial\psi_1}{\partial x}-g_{11}^{(2)}\frac{\partial^2 w}{\partial x^2}+g_{12}^{(1)}\frac{\partial\psi_2}{\partial y}-g_{12}^{(2)}\frac{\partial^2 w}{\partial y^2}\right)=0\end{cases}$$
$$y=0,\quad b:\begin{cases}\delta w=0\\ or\left(\begin{matrix}g_{22}^{(2)}\frac{\partial^2\psi_2}{\partial y^2}-g_{22}^{(3)}\frac{\partial^3 w}{\partial y^3}+g_{12}^{(2)}\frac{\partial^2\psi_1}{\partial x\partial y}-g_{12}^{(3)}\frac{\partial^3 w}{\partial x^2\partial y}\\ +S_{cyz}(\frac{\partial w}{\partial y}-\psi_2)\end{matrix}\right)=0\\ \delta\left(\frac{\partial w}{\partial y}\right)=0\\ or\left(-g_{22}^{(2)}\frac{\partial\psi_2}{\partial y}+g_{22}^{(3)}\frac{\partial^2 w}{\partial y^2}-g_{12}^{(2)}\frac{\partial\psi_1}{\partial x}+g_{12}^{(3)}\frac{\partial^2 w}{\partial x^2}\right)=0\\ \delta\psi_2=0\\ or\left(g_{22}^{(1)}\frac{\partial\psi_2}{\partial y}-g_{22}^{(2)}\frac{\partial^2 w}{\partial y^2}+g_{12}^{(1)}\frac{\partial\psi_1}{\partial x}-g_{12}^{(2)}\frac{\partial^2 w}{\partial x^2}\right)=0\end{cases}\qquad(11)$$

3. Solution method

Assuming that the sandwich plate is simply supported at all the edges, an analytical solution is proposed in the form of:

$$w(x,y)=\sum_{m,n}W_{mn}\,sin\frac{m\pi}{a}x\,sin\frac{n\pi}{b}y$$
$$\psi_1(x,y)=\sum_{m,n}\Psi_{1mn}\,cos\frac{m\pi}{a}x\,sin\frac{n\pi}{b}y\qquad(12)$$
$$\psi_2(x,y)=\sum_{m,n}\Psi_{2mn}\,sin\frac{m\pi}{a}x\,cos\frac{n\pi}{b}y$$

where *m* and *n* denote the number of half-waves in *x* and *y*-directions. The suggested solution satisfies the boundary conditions of Eq. (11). After inserting Eq. (12) into Eq. (10), the following equation is obtained.

$$\begin{bmatrix}k_{11}&k_{12}&k_{13}\\k_{21}&k_{22}&k_{23}\\k_{31}&k_{32}&k_{33}\end{bmatrix}\begin{bmatrix}W_{mn}\\\Psi_{1mn}\\\Psi_{2mn}\end{bmatrix}=\begin{bmatrix}0\\0\\0\end{bmatrix}\qquad(13)$$

where k_{ij} are can be found in Appendix 3. Now, a nontrivial solution is sought for Eq. (13).

$$det\begin{bmatrix}k_{11}&k_{12}&k_{13}\\k_{21}&k_{22}&k_{23}\\k_{31}&k_{32}&k_{33}\end{bmatrix}=0\qquad(14)$$

Solving Eq. (14) yields the following relation

$$C_1\Delta T+C_2N_x^r+C_3N_y^r=f_1-f_2\qquad(15)$$

where

$$C_1=(\frac{m\pi}{a})^2\tilde{N}_x^T+(\frac{n\pi}{b})^2\tilde{N}_y^T$$
$$C_2=-(\frac{m\pi}{a})^2$$
$$C_3=-(\frac{n\pi}{b})^2$$
$$f_1=(\frac{m\pi}{a})^4g_{11}^{(3)}+(\frac{m\pi}{a})^2(\frac{n\pi}{b})^2(2g_{12}^{(3)}+4g_{66}^{(3)})$$
$$+(\frac{n\pi}{b})^4g_{22}^{(3)}+(\frac{m\pi}{a})^2S_{cxz}+(\frac{n\pi}{b})^2S_{cyz}$$
$$f_2=\frac{(k_{12}^2k_{33}+k_{13}^2k_{22}-2k_{12}k_{13}k_{23})}{(k_{22}k_{33}-k_{23}^2)}\qquad(16)$$
$$\begin{pmatrix}\tilde{N}_x^T\\\tilde{N}_y^T\end{pmatrix}=\int_{-\frac{\hbar_c}{2}-\hbar_f}^{-\frac{\hbar_c}{2}}\begin{bmatrix}\bar{Q}_{11}&\bar{Q}_{12}\\\bar{Q}_{12}&\bar{Q}_{22}\end{bmatrix}_{face}\begin{Bmatrix}\alpha_x\\\alpha_y\end{Bmatrix}_{face}dz$$
$$+\int_{-\hbar_c/2}^{+\hbar_c/2}\begin{bmatrix}\bar{Q}_{11}&\bar{Q}_{12}\\\bar{Q}_{12}&\bar{Q}_{22}\end{bmatrix}_{core}\begin{Bmatrix}\alpha_x\\\alpha_y\end{Bmatrix}_{core}dz$$
$$+\int_{\hbar_c/2}^{\hbar_c/2+\hbar_f}\begin{bmatrix}\bar{Q}_{11}&\bar{Q}_{12}\\\bar{Q}_{12}&\bar{Q}_{22}\end{bmatrix}_{face}\begin{Bmatrix}\alpha_x\\\alpha_y\end{Bmatrix}_{face}dz$$

From Eq. (15), the buckling temperatures of the structure are calculated for different values of *m* and *n*. The minimum obtained value is considered as the critical buckling temperature, as denoted by the symbol of ΔT_{cr}.

4. Results and discussion

4.1 Verification study

Two comparative examples are provided to verify the accuracy of the proposed analytical method. In the first example, the critical buckling temperatures of a square sandwich plate with a soft-core and single-layered orthotropic face sheets $(0°/Core/0°)$ are obtained and compared with the results of Zhai *et al.* (2020). The material properties used in this example are as follows:

$Isotropic\ Core$:

$E=10MPa$, $\nu_{12}=0.3$, $\alpha=0.18\times10^{-6}{}^{o}\!/_{C}$

$Orthotropic\ Face\ sheets$:

$E_1=132GPa$, $E_2=10.3GPa$,
$G_{12}=6.5GPa\nu_{12}=0.3$,
$\alpha_1=1.2\times10^{-6}/^oC$, $\alpha_2=24\times10^{-6}/^oC$

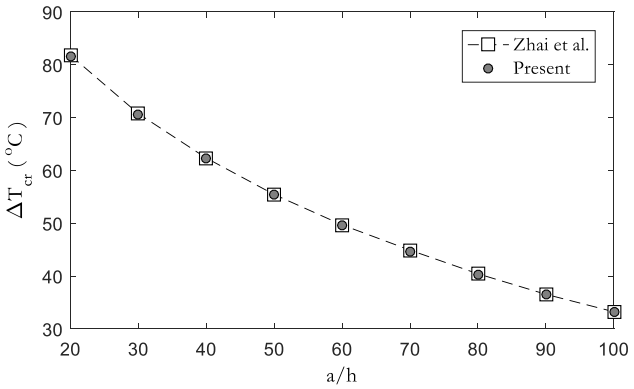

Fig. 2 The critical buckling temperatures of a sandwich plate with a soft-core and single-layer orthotropic face sheets ($a = b = 0.3m,\ h_f = 0.1mm$)

Table 1 The material properties of the NiTi wires used by Asadi *et al*. (2014)

Properties			
$M_f = 9°C$	$E_A = 67GPa$	$C_M = 8MPa/°C$	$\rho = 6450kg/m^3$
$M_s = 18.4°C$	$E_M = 26.3GPa$	$C_A = 13.8MPa/°C$	$\upsilon = 0.33$
$A_s = 34.5°C$	$\Theta = 0.55MPa/°C$	$\sigma_s^{cr} = 100MPa$	$\alpha_s = 10.26 \times 10^{-6}/°C$
$A_f = 49°C$		$\sigma_f^{cr} = 170MPa$	$\varepsilon_L = 0.067$

Table 2 The material properties of the composite used by Asadi *et al*. (2014)

Properties		
$E_{1m} = E_{1m}^0(1 + E_{1m}^1 \Delta T)$,	$E_{1m}^0 = 155GPa$,	$E_{1m}^1 = -3.53 \times 10^{-4}/°C$
$E_{2m} = E_{2m}^0(1 + E_{2m}^1 \Delta T)$,	$E_{2m}^0 = 8.07GPa$,	$E_{2m}^1 = -4.27 \times 10^{-4}/°C$
$G_{12m} = G_{12m}^0(1 + G_{12m}^1 \Delta T)$,	$G_{12m}^0 = 4.55GPa$,	$G_{12m}^1 = -6.06 \times 10^{-4}/°C$
$\alpha_{1m} = \alpha_{1m}^0(1 + \alpha_{1m}^1 \Delta T)$,	$\alpha_{1m}^0 = -0.07 \times 10^{-6}/°C$,	$\alpha_{1m}^1 = -1.25 \times 10^{-3}/°C$
$\alpha_{2m} = \alpha_{2m}^0(1 + \alpha_{2m}^1 \Delta T)$,	$\alpha_{2m}^0 = 30.1 \times 10^{-6}/°C$,	$\alpha_{2m}^1 = 0.41 \times 10^{-4}/°C$
$\upsilon_{12m} = 0.22$		

Table 3 The critical temperatures of a $[90°/0°/90°/0°]_s$composite plate with embedded SMA wires ($a/b = 1, a/h = 50, \varepsilon_0 = 0.01$

	V_s			
Ref.	0%	5%	10%	20%
Present	209.6	237.3	262.7	318.3
Asadi *et al*. (2014)*	206.3	232.0	259.0	313.1

* Data have been extracted from Fig. 12 of the research by Asadi *et al*. (2014) using a digitizing software

In Fig. 2, the critical buckling temperatures are plotted for different values of *a/h* ratio. As observed, the results obtained by the present study are very close to those reported by Zhai *et al*. (2020) with a negligible difference.

In the second example, the critical buckling temperatures of a laminated composite plate with embedded SMA wires in its outermost layers are calculated. The results are obtained for lamination scheme of$[90°_{SMA}/0°/90°/0°]_s$. To verify the present model, the structures can be assumed as a sandwich plate with 6-layer core with lay-up $[0°/90°/0°]_s$ and two 90° single layer face sheets with embedded SMA wires. The thermo-mechanical properties of the SMA wires and composite are tabulated in Tables 1 and 2. As observed from Table 3, the developed model in the present study can predict the buckling temperatures of laminated SMA hybrid composite plates with enough accuracy.

Based on the above two examples, the results of the present study are sufficiently accurate to estimate the thermal buckling behaviour of soft-core sandwich plates with hybrid SMA composite face sheets.

4.2 Thermal buckling of soft-core sandwich plates with advanced hybrid composite face sheets

In this subsection, the thermal buckling behavior of soft-core sandwich plates with GF/EP face sheets (see Fig. 1) is assessed. The composite face sheets may be reinforced with CNTs, SMA wires, or both. Before analyzing the structure, the following assumptions need to be considered:

• The material properties of the GF/EP composite without/with 0.3 wt% CNT are tabulated in Table 4, based on the authors' previous research.

• The material properties of SMA wires are listed in Table 5, based on Gao *et al*. (2006).

• The lamination scheme of the face sheets is assumed to be$[0°/90°/0°]_s$.

Table 4 Material properties of GF/EP composite free of CNT and with 0.3 wt% CNT (Kamarian *et al.* 2021)

Property	Unit	Composite type	
		GF/EP	CNT/GF/EP
E_1	GPa	129.62	129.74
E_2	GPa	7.23	7.71
G_{12}	GPa	2.71	2.89
υ_{12}	-	0.27	0.27
α_1	$10^{-6}/\ °C$	0.18	-0.02
α_2	$10^{-6}/\ °C$	29.13	21.7
T_g	$°C$	112.5	110.5

Table 5 Material properties of SMA wires (Gao *et al.* 2006)

Properties			
$M_f = 6.2°C$	$E_A = 27.17GPa$	$C_M = 8MPa/°C$	$\rho = 5719kg/m^3$
$M_s = 20.5°C$	$E_M = 13.58GPa$	$C_A = 13.8MPa/°C$	$\upsilon = 0.33$
$A_s = 53.6°C$	$\Theta = 0MPa/°C$	$\sigma_s^{cr} = 100MPa$	$\varepsilon_L = 0.067$
$A_f = 61.3°C$		$\sigma_f^{cr} = 170MPa$	

* The units have been converted to the metric system

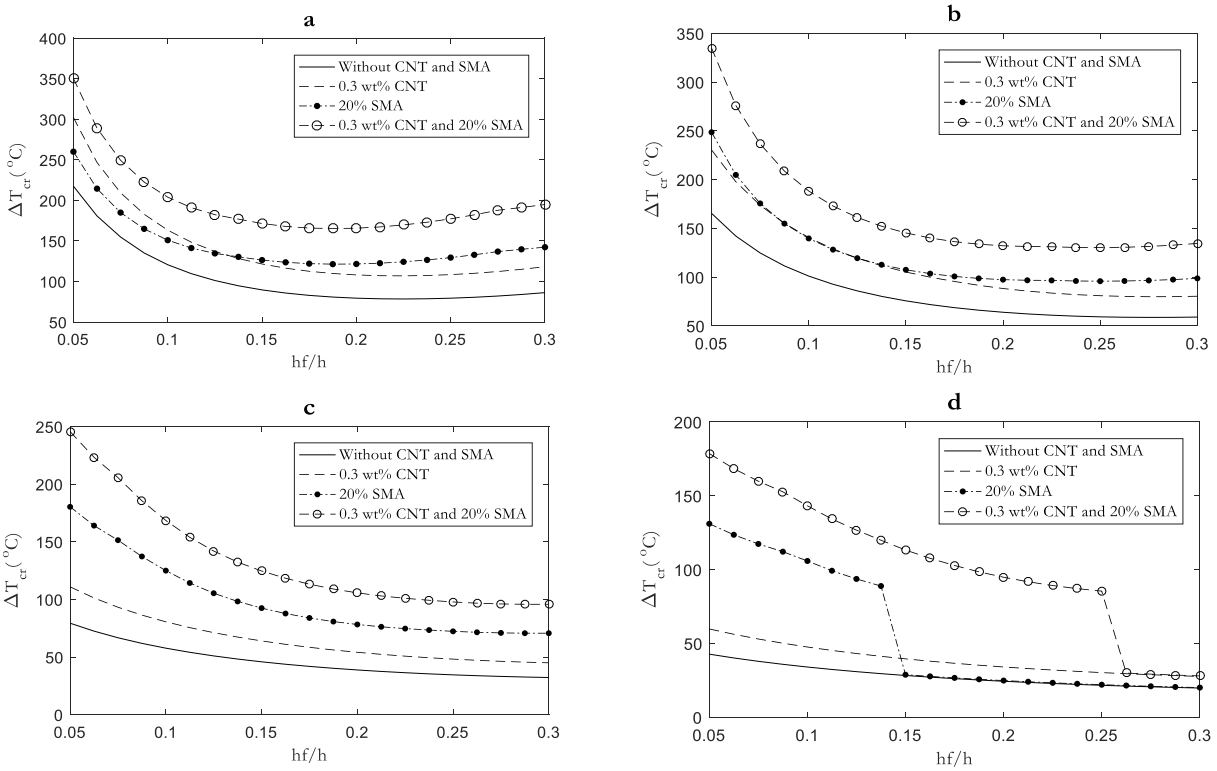

Fig. 3 The effects of different types of reinforcements in the GF/EP face sheets on the critical buckling temperatures of the sandwich plate ($a/b = 1$), a) $a/\hbar = 30$, b) $a/\hbar = 50$, c) $a/\hbar = 100$, d) $a/\hbar = 150$

Table 6 The effects of different types of reinforcement of the GF/EP face sheets on the critical buckling temperatures of the sandwich plate ($a/b = 1$)

$a/\hbar$	$\hbar_f/\hbar$	No reinforcement		CNT			SMA			CNT/SMA		
		$\Delta T(^\circ C)$	mode	$\Delta T(^\circ C)$	mode	Enhancement (%)	$\Delta T(^\circ C)$	mode	Enhancement (%)	$\Delta T(^\circ C)$	mode	Enhancement (%)
30	0.05	217.5	(1,1)	302.2	(1,2)	38.9	257.9	(1,6)	18.6	347.0	(1,6)	59.5
	0.1	120.7	(1,2)	163.3	(1,2)	35.3	151.0	(1,4)	25.1	204.0	(1,4)	69.0
	0.2	79.5	(1,2)	108.1	(1,2)	36.0	121.6	(1,3)	53.0	165.8	(1,3)	108.6
50	0.05	165.4	(1,1)	230.5	(1,1)	39.4	248.6	(1,4)	50.3	334.6	(1,5)	102.3
	0.1	101.1	(1,1)	140.6	(1,1)	39.1	138.4	(1,5)	36.9	186.5	(1,5)	84.5
	0.2	64.0	(1,1)	88.3	(1,2)	38.0	97.4	(1,4)	52.2	132.2	(1,4)	106.6
100	0.05	79.4	(1,1)	110.9	(1,1)	39.7	180.4	(1,2)	127.2	245.7	(1,2)	209.4
	0.1	57.7	(1,1)	80.6	(1,1)	39.7	125.0	(1,4)	116.6	168.5	(1,4)	192.0
	0.2	38.8	(1,1)	54.1	(1,1)	39.4	78.3	(1,5)	101.8	105.7	(1,5)	172.4
150	0.05	42.7	(1,1)	59.8	(1,1)	40.0	131.1	(1,2)	207.0	178.6	(1,2)	318.3
	0.1	34.0	(1,1)	47.6	(1,1)	40.0	105.9	(1,3)	211.5	143.2	(1,3)	321.2
	0.2	24.4	(1,1)	34.1	(1,1)	39.8	24.8	(1,1)	1.6	94.8	(1,5)	288.5

• SMA wires are assumed to be embedded in the outermost layers of the composite face sheets.

• The volume fraction and pre-strain value for the SMA wires are considered to be 20% and 1%, respectively, unless the values are mentioned.

• The material properties of the core are assumed to be as follows: $E = 10MPa, v = 0.3, \alpha = 0.18 \times 10^{-6}/^\circ C$

• For the sake of simplicity, the buckling temperature is considered as the difference between the temperature at which the structure buckles and the reference temperature ($\Delta T_{cr} = T - T_{ref}, T_{ref} = 20^\circ C$).

Table 6 presents the effects of different types of reinforcements in the face sheets on the critical buckling temperatures of the structure. The results are provided for various a/h and h_f/h ratios. As expected, with the increase of a/h ratio, the structure gets thinner, its total

stiffness decreases, and its buckling temperature declines. Furthermore, by enhancing h_f/h, the structure buckles at lower temperatures, which is not always the case as will be later shown in Fig. 3. Based on Table 6, CNTs enhance the critical buckling temperatures by about 35~40% at all a/h and h_f/h ratios. Therefore, CNTs have the advantage that they can lead to a relatively constant increase in buckling temperature, regardless of the geometry of the structure and the thickness of face sheets. Similar results (Kamarian *et al.* 2021) were observed for non-sandwich laminated composite plates where CNTs could increase the buckling temperature by 35 to 42%. Knowing that the glass transition temperature for the considered composite is about $112.5\,^{\circ}C$, ($\Delta T_g = T_g - T_{ref} = 92.5\,^{\circ}C$), incorporation of 0.3 wt% CNT to the face sheet of sandwich plates with buckling temperatures of $68.5\,^{\circ}C$ or higher can sufficiently postpone the buckling phenomenon to the glass transition temperature. On the other hand, such a constant improvement may not be efficient for the low critical buckling temperature of the base sandwich plate (without CNT and SMA in the face sheets). Concerning a sandwich plate with $a/h = 100$ and $h_f/h = 0.2$, the comparison indicates that CNTs can only increase the buckling temperature by $15.3\,^{\circ}C$ from $38.8\,^{\circ}C$ to $54.1\,^{\circ}C$. Another interesting point is that CNTs do not significantly alter the buckling modes of structure, and buckling occurs at $m = 1$, $n = 1$, 2 similar to the base sandwich plate.

Now, consider a sandwich plate whose composite face sheets are reinforced with SMA wires. Table 6 indicates that, unlike CNTs, SMA wires show a non-constant effect on the thermal stability of sandwich plates. For example, it may lead to 18.6% enhancement for the plate with $a/h = 30, h_f/h = 0.05$ but a 127.2% increment for the case with $a/h = 100$, $h_f/h = 0.05$. Thus, the performance of these wires highly depends on the geometry of the structures (a/h and h_f/h ratios). The important point is that embedding SMAs in the face sheets does not necessarily have a significant positive influence on the thermal buckling of the structure. Take a sandwich plate with $a/h = 150$ and $h_f/h = 0.2$ for example. If ΔT reaches $24.4\,^{\circ}C$, the base structure starts to buckle. In this case, embedding SMA wires does not affect the critical buckling temperature and ΔT_{cr} can change only around $0.4\,^{\circ}C$. This is because their critical buckling temperatures are lower than the austenite start temperature (see Table 5). This implies that buckling occurs before the martensite-austenite phase transition. Thus, the tensile recovery force is not generated by the SMAs to counteract the thermal compressive stress, and the little difference between the buckling temperatures can be assigned to the slight changes in the total stiffness and coefficient thermal expansion of the structure due to incorporation of 20% SMA in the outermost layers of the face sheets. Previous studies (Kamarian *et al.* 2020, 2022, Yas *et al.* 2021) showed that SMAs may even have a destructive effect on the thermal stability of composite beams, rectangular plates, and trapezoidal plates. Moreover, unlike CNTs, SMA wires may significantly affect the buckling modes. As observed, m and n can take different values from 1 to 6 which strongly depend on the geometric parameters. Another interesting conclusion is that although in some cases, using only SMA wires or CNTs does not notably affect the thermal stability of the plate, the simultaneous use of these materials may remarkably raise the critical buckling temperature. Again, consider a sandwich plate with $a/h = 150$ and $h_f/h = 0.2$. Based on Table 6, ΔT_{cr} is $34.1\,^{\circ}C$ and $24.8\,^{\circ}C$ for the GF/EP face sheets reinforced with 0.3 wt% and 20% SMA wires, respectively. However, the critical buckling temperature is $94.8\,^{\circ}C$ for sandwich plates with SMA/CNT/GF/EP face sheets. The reason is that in the latter case, CNTs can sufficiently enhance ΔT_{cr} to a temperature above A_s, therefore, SMAs can produce the recovery stress to further delay the buckling temperature. Similar results can be obtained from Fig. 3 regarding the variations of buckling temperature against a/h and h_f/h ratios. First, depending on a/h, the graphs may experience a downward-upward trend with the increase of face sheet thickness, i.e. an initial decline of the buckling temperature followed by an increment (see Fig. 3a). To explain this behavior, it should be noted that the total stiffness of the structure, as well as the generated thermal stress, enhance with the increase of face sheet thickness. Therefore, up to a certain value of h_f/h, the negative effect of thermal stress may be more dominant than the positive effect of the stiffness, hence, the buckling temperature decreases in the thicker face sheets. Similar behavior was predicted by Babu and Kant (2000) in studying the influence of face sheet thickness on the thermal buckling of sandwich plates. However, after that specific value of h_f/h, the effect of stiffness overcomes the effect of thermal environments, thus, the critical buckling temperature starts to increase with raising h_f/h ratio.

According to Fig. 3, depending on the geometric parameters, one of the CNTs and SMAs may outperform the other one. Fig. 3a is related to the sandwich plate with $a/h = 30$. As seen, the use of CNTs leads to better thermal stability when $h_f/h < 0.14$, but SMAs are preferable for the structure with thicker face sheets. For the case with $a/h = 50$ (see Fig. 3b), SMA wires and nanotubes have the same effects on the critical temperature when $0.008 < h_f/h < 0.014$ while SMAs are more powerful in enhancing ΔT_{cr} out of this thickness range. Fig. 3c for $a/h = 100$ indicates that SMAs play a more prominent role in increasing the buckling temperature at all h_f/h ratios. In the last case for $a/h = 150$, embedding SMAs in the GF/EP composite face sheets is effective only for $h_f/h < 0.014$, it is ineffectual for sandwich plates with thicker face sheets. In the mentioned h_f/h range, embedding SMAs can sufficiently delay the buckling temperature to temperatures above ΔT_g. Thus, unlike Fig. 3a, for sandwich plates with thinner face sheets, the use of shape memory wires takes precedence over CNTs. Despite the more dominant influence of CNTs for $a/h = 150$ and $h_f/h > 0.14$, the critical buckling temperature is not sufficiently increased in the presence of nanotubes as the power of CNTs to enhance buckling temperature is limited to around 35-40%. Thus, in such cases, none of the SMAs and CNTs are effective. Interestingly, co-incorporation of CNTs and SMAs leads to an astonishing enhancement in critical

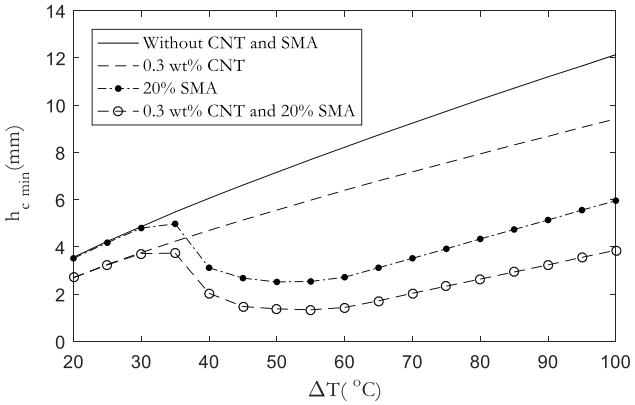

Fig. 4 Minimum required core thickness in the presence of different types of reinforcements in the face sheets under various operating temperatures ($a/b = 1$)

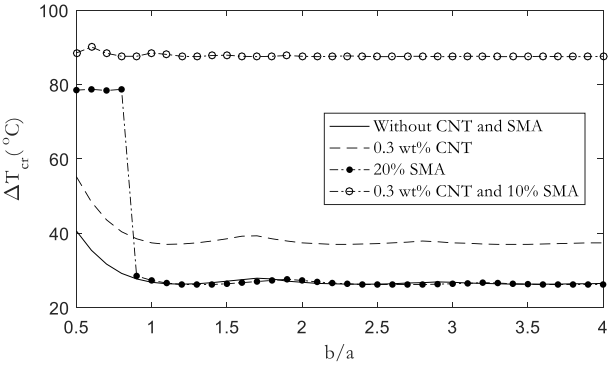

Fig. 5 The effects of different reinforcements in the face sheets on the variations of critical buckling temperatures against b/a parameter

temperature compared to the cases at which only one of CNTs or SMAs is used except for very thin plates with thick face sheets like when $\frac{a}{h} = 150,\ h_f/h > 0.25$. For $h_f/h > 0.25$, however, embedding SMAs does not affect the buckling temperatures even in the presence of CNTs since the buckling temperature of CNT-reinforced sandwich plates is still less thanA_s. Therefore, the graph for CNT-reinforced face sheets and SMA/CNT-reinforced face sheets are almost the same. In such situations, the use of only CNTs is preferable.

Here, the influence of CNTs and SMAs on the design of sandwich structures are addressed. The main purpose is to find the minimum required core thickness (h_{min}) to form a sandwich structure to withstand the thermal load and does not buckle. Fig. 4 shows the variations of h_{min} against the operating temperature. Note that the results of this figure ae obtained for face sheets with a thickness of 1 mm. As expected, for the sandwich plate whose GF/EP face sheets are neither reinforced with CNTs nor with SMAs, the required core thickness increases with the elevating the environmental temperature due to the generation of more compressive thermal stress at higher temperatures, therefore, the total stiffness of the structure needs to be increased. Then, a sandwich plate with CNT-reinforced face sheets is examined. Again, an increasing trend is observed for the variations of minimum allowable core thickness versus the operating temperature. However, the numerical results state that CNTs lead to structures requiring thinner cores to withstand buckling. A different trend is observed for the sandwich plate with SMA wire-embedded face sheets. The graph of this case follows an ascending-descending-ascending trend. Until $\Delta T = 35\ ^\circ C$, i.e., before the austenite temperature, the graph is almost the same as the case without CNTs and SMAs. For higher temperatures up to $75\ ^\circ C$ ($\Delta T = 55\ ^\circ C$), the SMAs begin to produce recovery stress, therefore, the structure requires a thinner core. By further temperature enhancement, the thermal stresses overcome the recovery stress, thus, thicker cores are needed. The sandwich plate with face sheets made of advanced hybrid SMA/CNT/GF/EP composite is also considered. The graph of this case exhibits an ascending-descending-ascending trend, similar to the previous case, except that the minimum required core thickness is lower as the structure takes the advantages of both CNTs and SMAs.

Finally, the effects of CNTs and SMAs on the variations of thermal buckling of sandwich plates are examined versus a/b parameter for $a/h = 150$, $h_f = 2mm$ and $h_f/h = 1/6$. Fig. 5 reveals that in the absence of CNTs and SMAs, the buckling temperature is about$40\ ^\circ C$at$b/a = 0.5$. Then, the diagram experiences a downward-upward trend with the increase of b/a parameter and finally converges to $26.5\ ^\circ C$. According to this figure, the incorporation of 0.3 wt% CNTs to the GF/EPP face sheets leads to a 35-40 % upward shift of the graph which eventually converges to $37\ ^\circ C$. For the sandwich plate with SMA wires in the outermost layers of face sheets ($V_s = 20\%$), the critical buckling temperatures are considerably enhanced only when $b/a < 0.8$. For plates with $b/a > 0.8$, the structure buckles before the SMA wires start to generate recovery stress. Therefore, the shape memory wires fail to change the graph of the base sandwich plate. Moreover, Fig. 5 depicts that the simultaneous use of 0.3 wt% CNTs and only 10% SMA wires in the face sheets gives rise to a superb performance. In this case, the buckling temperature is very close to the highest required value, i.e., ΔT_g at almost all values of b/a parameter.

5. Conclusions

The present work was mainly focused on the thermal buckling behavior of sandwich plates with advanced SMA/CNT hybrid composite face sheets. The stability equations were derived based on PLSDT and solved analytically for simply supported boundary conditions. Some conclusions of this study can be listed as:

• The developed analytical approach is simple but accurate enough to predict the thermal buckling behavior of sandwich plates made of soft cores and advanced hybrid SMA/CNT composite fac sheets.

• CNTs have an almost constant (35~40%) positive effect on the critical buckling temperatures (ΔT_{cr}) of sandwich structures regardless of the geometric parameters and operating temperature.

• For base sandwich plates whose buckling temperature

is around 68 ℃ or more, 0.3 %wt CNTs can sufficiently delay the ΔT_{cr} to its highest required level (ΔT_g).

• CNTs do not change the buckling modes (m, n) significantly.

• The influence of SMAs on the thermal stability of sandwich plates is highly variable and depends on the geometry of the structure and working temperature.

• For sandwich plates with high a/h or b/a ratios, SMAs were not effective to enhance the buckling temperatures.

• Embedding SMA wires is almost ineffective if the base sandwich plates are used at low-temperature environments ($T < A_s$) or when their buckling temperature is less than A_s.

• SMAs may considerably change the buckling modes.

• Depending on b/a,a/h,h_f/h ratios and the working temperature, using one of the CNTs and SMAs may lead to stronger performance compared to the other.

• In some cases (like $\frac{b}{a} = 1$, $\frac{a}{h} = 50, 0.08 < h_f/h < 0.14$), CNTs and SMAs have almost the same impact on the critical buckling temperatures of the structure.

• In some cases, using only one of the CNTs or SMAs does not remarkably alter the buckling temperature, while their simultaneous application significantly enhances the thermal stability of the structure.

• The co-presence of SMAs and CNTs does not necessarily lead to superb enhancement in the buckling temperatures at all conditions. For plates with a high b/a ratio, no meaningful difference is observed between the ΔT_{cr} of sandwich plates reinforced by only CNTs and those reinforced by both CNTs and SMAs.

Selecting proper reinforcement can considerably decrease the required core thickness and therefore the weight of sandwich plates

Acknowledgments

This study was supported by the Basic Science Research Program through the National Research Foundation of Korea (NRF) funded by the Ministry of Science Education (2018R1A6A1A03024509 and 2021R1A2B5B03002355)

References

Asadi, H., Akbarzadeh, A.H., Chen, Z.T. and Aghdam, M.M (2015), "Enhanced thermal stability of functionally graded sandwich cylindrical shells by shape memory alloys", *Smart Mater. Struct.*, **24**(4), 045022. https://doi.org/10.1088/0964-1726/24/4/045022.

Babu, C.S. and Kant, T. (2000), "Refined higher order finite element models for thermal buckling of laminated composite and sandwich plates", *J. Therm. Stress.*, **23**(2), 111-130. https://doi.org/10.1080/014957300280489.

Barai, P. and Weng G.J. (2011), "A theory of plasticity for carbon nanotube reinforced composites", *Int. J. Plast.*, **27** (4), 539-559. https://doi.org/10.1016/j.ijplas.2010.08.006.

Bendenia, N., Zidour, M., Bousahla A.A, Bourada F., Tounsi, A., Benrahou, K.H., Adda Bedia E.A., Mahmoud, S.R. and Tounsi, A. (2020), "Deflections, stresses and free vibration studies of FG-CNT reinforced sandwich plates resting on Pasternak elastic foundation", *Comput. Concr.*, **26**(3), 213-226. https://doi.org/10.12989/cac.2020.26.3.213.

Bhaskar, J., Sharma A.K., Bhattacharya B. and Adhikari, S. (2020), "A review on shape memory alloy reinforced polymer composite materials and structures", *Smart Mater. Struct.*, **29**(7), 073001. https://doi.org/10.1088/1361-665X/ab8836.

Birman, V. and G.A. Kardomateas (2018), "Review of current trends in research and applications of sandwich structures", *Compos. Part B Eng.*, **142**, 221-240. https://doi.org/10.1016/j.compositesb.2018.01.027.

Brinson, L.C. (1993), "One-dimensional constitutive behavior of shape memory alloys: Thermomechanical derivation with non-constant material functions and redefined martensite internal variable," *J. Intell. Mater. Syst. Struct.*, **4**(2), 229-242. https://doi.org/10.1177%2F1045389X9300400213.

Daikh, A.A., Drai, A., Bensaid, I., Houari M.S.A. and Tounsi, A. (2021), "On vibration of functionally graded sandwich nanoplates in the thermal environment", *J. Sandw. Struct. Mater.*, **23**(6), 2217-2244. https://doi.org/10.1177%2F1099636220909790.

Dat, Ngo Dinh, Tran Quoc Quan, and Nguyen Dinh Duc. (2021), "Nonlinear thermal dynamic buckling and global optimization of smart sandwich plate with porous homogeneous core and carbon nanotube reinforced nanocomposite layers", *Eur. J. Mech. A Solids*, **90**, 104351. https://doi.org/10.1016/j.euromechsol.2021.104351.

Ebrahimi, F. and Farazmandnia N. (2018), "Thermal buckling analysis of functionally graded carbon nanotube-reinforced composite sandwich beams", *Steel Compos. Struct.*, **27**(2), 149-159. https://doi.org/10.12989/scs.2018.27.2.149.

Gao, X., Burton, D., Turner T. L. and Brinson L. C. (2006), "Finite element analysis of adaptive-stiffening and shape-control SMA hybrid composites", *Smart Struct. Mater.*, **5761**, 406-416. https://doi.org/10.1115/1.2203108.

Garg, A., Chalak, H.D., Belarbi, M.O., Zenkour, A.M. and Sahoo, R. (2021), "Estimation of carbon nanotubes and their applications as reinforcing composite materials–an engineering review", *Compos. Struct.*, **272**, 114234. https://doi.org/10.1016/j.compstruct.2021.114234.

Kamarian, S., Bodaghi, M., Barbaz-Isfahani R. and Song, J-I (2020), "A comparison between the effects of shape memory alloys and carbon nanotubes on the thermal buckling of laminated composite beams", *Mech. Based Des. Struct.*, 1-24. https://doi.org/10.1080/15397734.2020.1776131.

Kamarian, S., Bodaghi M., Barbaz Isfahani, R. Shakeri M. and Yas, M.H. (2021a), "Influence of carbon nanotubes on thermal expansion coefficient and thermal buckling of polymer composite plates: Experimental and numerical investigations", *Mech. Based Des. Struct.*, **49**(2), 217-232. https://doi.org/10.1080/15397734.2019.1674664.

Kamarian, S., Bodaghi, M., Barbaz—Isfahani R. and Song, J.I. (2021b), "Thermal buckling analysis of sandwich plates with soft-core and CNT-Reinforced composite face sheets", *J. Sandw. Struct. Mater.*, **23**(8), 3606-3644. https://doi.org/10.1177%2F1099636220935557.

Kamarian, S. and Song J.I. (2022), "Thermal buckling of advanced hybrid composite plates in the co-presence of CNTs and SMAs", *Mech. Adv. Mater. Struct.*, Published online. https://doi.org/10.1080/15376494.2021.2023921.

Katariya, P.V., Panda S.K., Hirwani C.K., Mehar K. and Thakare, O. (2017), "Enhancement of thermal buckling strength of laminated sandwich composite panel structure embedded with shape memory alloy fibre", *Smart Struct. Syst.*, **20** (5), 595-605.

Lal, A. and Markad K. (2021), "Thermal post buckling analysis of smart SMA hybrid sandwich composite plate", *Polym. Polym. Compos.*, **29**(9), S344-S360.

https://doi.org/10.1177%2F09673911211001276.
Lecce, L. and Concilio, A. (2015), *Shape Memory Alloy Engineering: For Aerospace, Structural and Biomedical Applications*, Elsevier, New York, U.S.A.
Li, X., Yu, K., Han J., Zhao R. and Wu, Y. (2015), "A piecewise shear deformation theory for free vibration of composite and sandwich panels", *Compos. Struct.*, **124**, 111-119. https://doi.org/10.1016/j.compstruct.2015.01.007.
Li, X., Yu, k. and Zhao, R. (2018), "Thermal post-buckling and vibration analysis of a symmetric sandwich beam with clamped and simply supported boundary conditions", *Arch. Appl. Mech.*, **88**(4), 543-561. https://doi.org/10.1007/s00419-017-1326-x.
Mehar, K., Panda,S. K., Devarajan Y. and Choubey G. (2019), "Numerical buckling analysis of graded CNT-reinforced composite sandwich shell structure under thermal loading", *Compos. Struct.*, **216**, 406-414. https://doi.org/10.1016/j.compstruct.2019.03.002.
Mekerbi, M., Benyoucef, S., Mahmoudi, A., Tounsi, A., Bousahla, A.A. and Mahmoud, S.R. (2021), "Thermodynamic behavior of functionally graded sandwich plates resting on different elastic foundation and with various boundary conditions", *J. Sandw. Struct. Mater.*, **23**(3), 1028-1057. https://doi.org/10.1177%2F1099636219851281.
Nejati, M., Ghasemi-Ghalebahman A., Soltanimaleki A., Dimitri R. and Tornabene, F. (2019), "Thermal vibration analysis of SMA hybrid composite double curved sandwich panels", *Compos. Struct.*, **224**, 111035. https://doi.org/10.1016/j.compstruct.2019.111035.
Reddy, J.N. (2003), *Mechanics of Laminated Composite Plates and Shells: Theory and Analysis*, CRC press, Boca Raton.
Sankar, A., Natarajan S., Merzouki T. and Ganapathi M. (2017), "Nonlinear dynamic thermal buckling of sandwich spherical and conical shells with CNT reinforced facesheets", *Int. J. Struct. Stabil. Dyn.*, **17**(9), 1750100. https://doi.org/10.1142/S0219455417501000.
Siddiqui, N.A., Li, E.L., Sham, M.L., Tang, B.Z. Gao, S.L., Mäder, E. and Kim J.K. (2010), "Tensile strength of glass fibres with carbon nanotube–epoxy nanocomposite coating: effects of CNT morphology and dispersion state", *Compos. Part A*, **41**(4), 539-548. https://doi.org/10.1016/j.compositesa.2009.12.011.
Tsoi, K.A., Stalmans, R., Schrooten, J., Wevers, M. and Mai, Y.W. (2003), "Impact damage behaviour of shape memory alloy composites", *Mater. Sci. Eng. A*, **342**(1-2), 207-215. https://doi.org/10.1016/S0921-5093(02)00317-9.
Tung H.V. and Long, V.T. (2019) "Buckling and postbuckling of CNT-reinforced composite sandwich cylindrical panels subjected to axial compression in thermal environments", *Vietnam J. Mech.*, **41**(3), 217-231. https://doi.org/10.15625/0866-7136/13673.
Watanabe, N., Sato, H. and Hishi, Y. (1997), "Thermal buckling behavior in Al honeycomb sandwich plates with very thin cfrp faces", *Proceedings of the 38th Structures, Structural Dynamics, And Materials Conference*, Kissimmee, FL, U.S.A., April.
Yas, M.H., Basati F. and Kamarian, S. (2021), "Thermal buckling of trapezoidal composite laminated plates with embedded shape memory alloys", *Polym. Compos.*, **42**(7), 3349-3362. https://doi.org/10.1002/pc.26063.
Zhai, Y., Su, J. and Liang, S. (2020), "Free vibration and buckling analysis of composite sandwich plates in thermal environment", *J. Sandw. Struct. Mater.*, **22**(8), 2604-2628. https://doi.org/10.1177%2F1099636218795375.

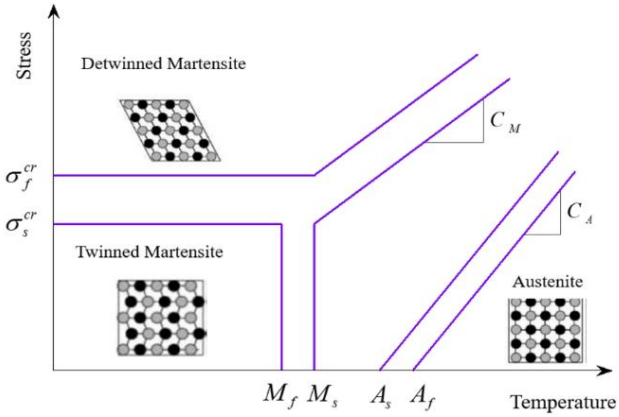

Fig. A1 Schematic phase diagram for SMAs (Kamarian and Song 2022)

Appendix 1

The unique properties of SMAs can be assigned to the phase transformation of austenite to martensite and vice versa upon exposure to thermo-mechanical loads (see Fig. A1). In the absence of mechanical load, there are four important temperatures for SMAs, which are the martensite start (M_s), martensite finish (M_f), austenite start (A_s) and austenite finish (A_f). Furthermore, by applying a mechanical force, the conversion to detwinned martensite can occur in SMAs, in which, the critical stresses for the start and end of this conversion are constant when $T < M_s$ and almost linear when $T > M_s$ (see the slopes of curves in Fig. A1 shown by C_M and C_A). According to the Brinson's findings, the martensite volume fraction of SMAs can be divided into two parts of stress-induced martensite (ξ_s) and temperature-induced martensite (ξ_T), namely (Brinson, 1993):

$$\xi = \xi_s + \xi_T \tag{A1}$$

Brinson (1993) indicated that the recovery stress generated by SMAs can be obtained based on the following equation.

$$\sigma = E_s(\xi)(\varepsilon - \varepsilon_L \xi_s) + \Theta \Delta T \tag{A2}$$

where E_s, ε_L, Θ and ΔTdenote the Young's modulus of SMAs, maximum residual strain, thermo-elastic tensor, and the temperature variations, respectively. In addition, $E_s$can be calculated by:

$$E_s(\xi) = \frac{E_A}{1 + \left(\frac{E_A}{E_M} - 1\right)\xi} \tag{A3}$$

in which, E_A and E_M refer to the Yong's modulus of SMAs at pure austenite and martensite phases, respectively. Based on the research performed by Brinson (1993), for the region at which $T > A_s$ and $C_A(T - A_f) < \sigma < C_A(T - A_s)$, the martensite fraction during heating can be obtained by:

$$\xi = \frac{\xi_0}{2}\left\{cos\left[\frac{\pi}{A_f - A_s}\left(T - A_s - \frac{\sigma}{C_A}\right)\right] + 1\right\} \tag{A4}$$

$$\xi_s = \xi_{s0}\frac{\xi}{\xi_0}, \xi_T = \xi_{T0}\frac{\xi}{\xi_0}$$

In which, the subscript '0' shows the initial state of the parameters. More details about SMAs features and behavior can be found elsewhere (Brinson 1993, Lecce and Concilio 2015, Bhaskar *et al.* 2020).

Appendix 2

$$g_{11}^{(1)} = 2(\frac{h_c+h_f}{2})^2 A_{11}^f + (\frac{h_c+h_f}{h_c})^2 D_{11}^c \quad , \quad g_{22}^{(1)} = 2(\frac{h_c+h_f}{2})^2 A_{22}^f + (\frac{h_c+h_f}{h_c})^2 D_{22}^c$$

$$g_{12}^{(1)} = 2(\frac{h_c+h_f}{2})^2 A_{12}^f + (\frac{h_c+h_f}{h_c})^2 D_{12}^c \quad , \quad g_{66}^{(1)} = 2(\frac{h_c+h_f}{2})^2 A_{66}^f + (\frac{h_c+h_f}{h_c})^2 D_{66}^c$$

$$g_{11}^{(2)} = (\frac{h_f}{h_c})(\frac{h_c+h_f}{h_c}) D_{11}^c \quad , \quad g_{22}^{(2)} = (\frac{h_f}{h_c})(\frac{h_c+h_f}{h_c}) D_{22}^c$$

$$g_{12}^{(2)} = (\frac{h_f}{h_c})(\frac{h_c+h_f}{h_c}) D_{12}^c \quad , \quad g_{66}^{(2)} = (\frac{h_f}{h_c})(\frac{h_c+h_f}{h_c}) D_{66}^c$$

$$g_{11}^{(3)} = 2D_{11}^f + (\frac{h_f}{h_c})^2 D_{11}^c \quad , \quad g_{22}^{(3)} = 2D_{22}^f + (\frac{h_f}{h_c})^2 D_{22}^c$$

$$g_{12}^{(3)} = 2D_{12}^f + (\frac{h_f}{h_c})^2 D_{12}^c \quad , \quad g_{66}^{(3)} = 2D_{66}^f + (\frac{h_f}{h_c})^2 D_{66}^c$$

where A_{fij}, A_{cij}, D_{fij} and D_{cij} denote the extensional stiffness coefficients of the face sheets, extensional stiffness coefficients of the core, bending stiffness coefficients of the face sheets and bending stiffness coefficients of the core, respectively, defined by:

$$(A_{fij}, D_{fij}) = \int_{h_c/2}^{h_c/2+h_f} \bar{Q}_{ij_{face}} \left[1, \left(z - \frac{h_c+h_f}{2}\right)^2\right] dz = \int_{-h_c/2-h_f}^{-h_c/2} \bar{Q}_{ij_{face}} \left[1, \left(z + \frac{h_c+h_f}{2}\right)^2\right] dz$$

$$(A_{cij}, D_{cij}) = \int_{-h_c/2}^{h_c/2} \bar{Q}_{ij_{core}} (1, z^2) dz$$

Appendix 3

$$k_{11} = (\frac{m\pi}{a})^4 g_{11}^{(3)} + (\frac{m\pi}{a})^2 (\frac{n\pi}{b})^2 (2g_{12}^{(3)} + 4g_{66}^{(3)}) + (\frac{n\pi}{b})^4 g_{22}^{(3)} + (\frac{m\pi}{a})^2 (S_{cxz} + N_x^r - N_x^T) + (\frac{n\pi}{b})^2 (S_{cyz} + N_y^r - N_y^T)$$

$$k_{12} = -(\frac{m\pi}{a})^3 g_{11}^{(2)} - (\frac{m\pi}{a})(\frac{n\pi}{b})^2 (g_{12}^{(2)} + 2g_{66}^{(2)}) - (\frac{m\pi}{a}) S_{cxz}$$

$$k_{13} = -(\frac{n\pi}{b})^3 g_{22}^{(2)} - (\frac{m\pi}{a})^2 (\frac{n\pi}{b})(g_{12}^{(2)} + 2g_{66}^{(2)}) - (\frac{n\pi}{b}) S_{cyz}$$

$$k_{21} = k_{12}$$

$$k_{22} = (\frac{m\pi}{a})^2 g_{11}^{(1)} + (\frac{n\pi}{b})^2 g_{66}^{(1)} + S_{cxz}$$

$$k_{23} = (\frac{m\pi}{a})(\frac{n\pi}{b})(g_{12}^{(1)} + g_{66}^{(1)})$$

$$k_{31} = k_{13}$$

$$k_{32} = k_{23}$$

$$k_{33} = (\frac{n\pi}{b})^2 g_{22}^{(1)} + (\frac{m\pi}{a})^2 g_{66}^{(1)} + S_{cyz}$$